Variation of $k_{Q_{clin},Q_{msr}}^{f_{clin},f_{msr}}$ for the small-field dosimetric parameters percentage depth dose, tissue-maximum ratio, and off-axis ratio

Paolo Francescon[a)]
Department of Radiation Oncology, Ospedale Di Vicenza, Viale Rodolfi, Vicenza 36100, Italy

Sam Beddar
Department of Radiation Physics, The University of Texas MD Anderson Cancer Center, Houston, Texas 77005

Ninfa Satariano
Department of Radiation Oncology, Ospedale Di Vicenza, Viale Rodolfi, Vicenza 36100, Italy

Indra J. Das
Department of Radiation Oncology, Indiana University School of Medicine, Indianapolis, Indiana 46202

(Received 1 April 2014; revised 25 August 2014; accepted for publication 31 August 2014; published 30 September 2014)

Purpose: Evaluate the ability of different dosimeters to correctly measure the dosimetric parameters percentage depth dose (PDD), tissue-maximum ratio (TMR), and off-axis ratio (OAR) in water for small fields.
Methods: Monte Carlo (MC) simulations were used to estimate the variation of $k_{Q_{clin},Q_{msr}}^{f_{clin},f_{msr}}$ for several types of microdetectors as a function of depth and distance from the central axis for PDD, TMR, and OAR measurements. The variation of $k_{Q_{clin},Q_{msr}}^{f_{clin},f_{msr}}$ enables one to evaluate the ability of a detector to reproduce the PDD, TMR, and OAR in water and consequently determine whether it is necessary to apply correction factors. The correctness of the simulations was verified by assessing the ratios between the PDDs and OARs of 5- and 25-mm circular collimators used with a linear accelerator measured with two different types of dosimeters (the PTW 60012 diode and PTW PinPoint 31014 microchamber) and the PDDs and the OARs measured with the Exradin W1 plastic scintillator detector (PSD) and comparing those ratios with the corresponding ratios predicted by the MC simulations.
Results: MC simulations reproduced results with acceptable accuracy compared to the experimental results; therefore, MC simulations can be used to successfully predict the behavior of different dosimeters in small fields. The Exradin W1 PSD was the only dosimeter that reproduced the PDDs, TMRs, and OARs in water with high accuracy. With the exception of the EDGE diode, the stereotactic diodes reproduced the PDDs and the TMRs in water with a systematic error of less than 2% at depths of up to 25 cm; however, they produced OAR values that were significantly different from those in water, especially in the tail region (lower than 20% in some cases). The microchambers could be used for PDD measurements for fields greater than those produced using a 10-mm collimator. However, with the detector stem parallel to the beam axis, the microchambers could be used for TMR measurements for all field sizes. The microchambers could not be used for OAR measurements for small fields.
Conclusions: Compared with MC simulation, the Exradin W1 PSD can reproduce the PDDs, TMRs, and OARs in water with a high degree of accuracy; thus, the correction used for converting dose is very close to unity. The stereotactic diode is a viable alternative because it shows an acceptable systematic error in the measurement of PDDs and TMRs and a significant underestimation in only the tail region of the OAR measurements, where the dose is low and differences in dose may not be therapeutically meaningful. [http://dx.doi.org/10.1118/1.4895978]

Key words: small beams, correction factor, output factor, Monte Carlo, detector

1. INTRODUCTION

Dosimetric parameters such as percent depth dose (PDD), tissue-maximum ratio (TMR), and off-axis ratio (OAR)[1] are used for radiation dosimetry and treatment planning. They are defined as

$$\mathrm{PDD}(z,f_{clin},F)=\frac{D(z,f_{clin},F)}{D(z_{max},f_{clin},F)}, \quad (1)$$

$$\mathrm{TMR}(z,f_{clin})=\frac{D(z,f_{clin})}{D(z_{max},f_{clin})}, \quad (2)$$

$$\mathrm{OAR}(r,z,f_{clin})=\frac{D(0,z,f_{clin})}{D(r,z,f_{clin})}, \quad (3)$$

where z is the depth, z_{max} is the depth of maximum dose, r is the distance from the central axis of the beam, F is the source-to-surface distance, and f_{clin} is the clinical field.

These parameters, which are well defined in most textbooks, are the ratios of two doses and are measured routinely for every machine for a wide range of field sizes as described in the report of Task Group 106 of the Therapy Physics Committee of the American Association of Physicists in Medicine.[2] In modern radiotherapy, small photon fields smaller than 3×3 cm are commonly used, especially in procedures such as intensity-modulated radiotherapy (IMRT), stereotactic body radiotherapy, Gamma Knife radiosurgery, and CyberKnife radiosurgery. The framework of small-field reference dosimetry has been presented by Alfonso *et al.*,[3] and its implications in relative dosimetry have been presented in many publications.[4,5] In the International Atomic Energy Agency–American Association of Physicists in Medicine Task Group's report,[3] the absorbed dose D to water at a point in a phantom in the absence of a dosimeter for a clinical field is defined as

$$D^{f_{clin}}_{w,Q_{clin}} = D^{f_{msr}}_{w,Q_{msr}} \Omega^{f_{clin},f_{msr}}_{Q_{clin},Q_{msr}}, \quad (4)$$

where f_{clin}, Q_{clin}, f_{msr}, and Q_{msr} are the clinical field, the clinical field's beam quality, the machine-specific reference field, and the machine-specific reference field's beam quality, respectively. A field factor, $\Omega^{f_{clin},f_{msr}}_{Q_{clin},Q_{msr}}$, converts the absorbed dose to water per monitor unit (MU) for the machine-specific reference field to the absorbed dose to water per MU in the clinical field. The field factor can be determined as the ratio of detector readings multiplied by a detector correction factor, $k^{f_{clin},f_{msr}}_{Q_{clin},Q_{msr}}$. For the sake of simplicity, we define k_Ω as

$$k_\Omega \equiv k^{f_{clin},f_{msr}}_{Q_{clin},Q_{msr}} = \frac{\left(D^{f_{clin}}_{w,Q_{clin}}\right)/\left(M^{f_{clin}}_{Q_{clin}}\right)}{\left(D^{f_{msr}}_{w,Q_{msr}}\right)/\left(M^{f_{msr}}_{Q_{msr}}\right)}, \quad (5)$$

where M and D are the readings per MU of the detector corrected for influence quantities and dose, respectively. The factor k_Ω accounts for the difference between the detector response in the fields f_{clin} and f_{msr} and can be calculated using Monte Carlo (MC) simulation if we assume that the reading of the detector corrected for influence quantities is proportional to the dose absorbed in the sensitive volume.[5]

However, most of the current literature fails to discuss the impact of k_Ω on dosimetric parameters except the output factor (OF), especially in relation to the microchambers that are being marketed by most vendors. Notwithstanding the fact that manufacturers are making microdetectors for use in small fields, the response of the detectors warrants investigation. The detectors produced within the last few years have become increasingly smaller but produce significant fluence perturbations owing to the similar dimensions of the sensitive volume with respect to the field size. In addition, the presence of non-water-equivalent materials surrounding the sensitive volume and reduced signal-to-noise ratio due to the smaller sensitive volume needs further investigation.

There are several challenges in the dosimetry of small fields arising primarily from the occlusion of the direct photon beam source owing to small collimator settings and the lack of lateral charged particle equilibrium, as shown by Das *et al.*[6] Moreover, in small fields with sharp dose gradients and steep falloff in the dose profiles with relatively little flatness in the field center, most widely available detectors are too large to provide accurate dosimetric parameters. To a lesser extent, variations in radiological parameters due to changes in the particle spectrum with decreasing field size also need to be considered. Numerous experiments and MC simulations[7–16] have been performed to investigate the suitability of the various types of detectors for measuring PDD, TMR, OAR, and OF in small photon fields. However, most of these studies lack a detailed analysis of the behavior of the available dosimeters that would enable one to make an informed choice of an appropriate detector in terms of size, composition, and construction.

MC has proven to be an effective tool to calculate the k_Ω correction factor $k^{f_{clin},f_{ref}}_{Q_{clin},Q_{ref}}$.[17–23] In particular, with MC it is possible to very accurately simulate detectors in terms of their design, materials, and composition and calculate with high accuracy both the dose deposited within the cavity or sensitive volume and the perturbation correction factors of dosimeters in nonreference conditions.[24–28]

Previously, MC simulation of dose to water and dose to detector has been used to calculate the correction factors needed for dose calibration and OF measurements on the CyberKnife system[18,19] and standard Linacs.[17] In the present study, we used MC simulations to estimate the variation of k_Ω of several types of dosimeters (stereotactic diodes, microchambers, microLion, and plastic scintillator detectors [PSDs]) as a function of depth for the PDD and the TMR measurements and as a function of the distance from the central axis of the beam for the OAR measurements. The variation of k_Ω enables one to evaluate the ability of a detector to reproduce the PDDs, TMRs, and OARs in water and consequently determine whether it is necessary to apply correction factors. Moreover, if different depths for dose calibration and OF measurements are used with respect to those indicated in references,[18,19] the correct k_Ω can be selected by the user. We verified the correctness of the simulations by comparing the experimental percentage differences between the PDDs and OARs obtained using the PTW 60012 diode and the PTW PinPoint 31014 microchamber and the PDDs and OARs obtained using the Exradin W1 PSD for 5- and 25-mm collimators with those predicted by the MC simulations. We used the Exradin W1 PSD as a reference because its sensitive volume is very small (1 mm diameter × 3 mm length) and made from a water-equivalent plastic scintillator and because the whole system is made from materials that can be considered water-equivalent; in principle, the detector does not perturb the electron fluence in water. PSDs have been well studied and shown to respond linearly to absorbed dose, and they are dose rate- and energy-independent.[29,30]

We evaluated the dependence of k_Ω on field size, position, and depth in the context of PDD, TMR, and OAR for very small fields from a CyberKnife system using MC simulation for various commercially available detectors. We did not evaluate OF, as it has been investigated thoroughly by various other researchers.[11,18,19,31,32]

2. MATERIALS AND METHODS

2.A. MC simulations

The CyberKnife system delivering 6-MV photon beam was modeled using the BEAMnrc code.[33] The actual geometry and material composition of the detectors were modeled using the `egs_chamber` code.[34] MC simulations were performed to determine the correction factors, defined as

$$k_{\Omega}(0,z,\mathrm{PDD}) = \frac{(D(0,z,f_{\mathrm{clin}})_w)\cdot(D(0,z_{\mathrm{ref}},f_{\mathrm{msr}})_{\mathrm{det}})}{(D(0,z,f_{\mathrm{clin}})_{\mathrm{det}})\cdot(D(0,z_{\mathrm{ref}},f_{\mathrm{msr}})_w)}, \quad (6)$$

$$k_{\Omega}(0,z,\mathrm{TMR}) = \frac{(D(0,z,f_{\mathrm{clin}})_w)\cdot(D(0,z_{\mathrm{ref}},f_{\mathrm{msr}})_{\mathrm{det}})}{(D(0,z,f_{\mathrm{clin}})_{\mathrm{det}})\cdot(D(0,z_{\mathrm{ref}},f_{\mathrm{msr}})_w)}, \quad (7)$$

$$k_{\Omega}(r,z,\mathrm{OAR}) = \frac{(D(r,z,f_{\mathrm{clin}})_w)\cdot(D(0,z_{\mathrm{ref}},f_{\mathrm{msr}})_{\mathrm{det}})}{(D(r,z,f_{\mathrm{clin}})_{\mathrm{det}})\cdot(D(0,z_{\mathrm{ref}},f_{\mathrm{msr}})_w)}, \quad (8)$$

where $D(r,z)$ represents the total dose per initial history scored within the sensitive volume of the modeled detector in water at depth z and distance r from the central axis of the beam. Complete descriptions of the methodology used to calculate these correction factors have been published previously.[17–19] As has been previously reported,[5,17] we assumed that the reading of the detector corrected for factors such as polarity effect, dose-rate dependence, and temperature dependence was proportional to the dose absorbed in the sensitive volume. Therefore, $k_{\Omega}(0,z,\mathrm{PDD})$, $k_{\Omega}(0,z,\mathrm{TMR})$, and $k_{\Omega}(r,z,\mathrm{OAR})$, were computed using MC simulation. The geometry and composition of the detectors were obtained from the technical sketches provided by the manufacturer. For the CyberKnife system, the source-to-detector distance was 80 cm, z_{ref} was 1.5 cm, and f_{msr} was a circular field 60 mm in diameter.

The `egs_chamber` user code[35,36] was used to simulate $D(r,z)$. The cross-section enhancement factor was set to 2048 in a volume extending 1.5 cm around the sensitive volume for depths greater than 1.5 cm; in the buildup region, the thickness of the volume in front of the sensitive volume of the detector was the distance to the surface of the phantom. The cross-section enhancement volume included the air between the phantom and the beam source. The EGSnrc cross-section options and transport parameters were set to the default values. The particle production and transport threshold energies were 521 keV (e^+/e^-) and 10 keV (gamma). To calculate the doses at different depths or at different distances from the central axis within a single simulation, we used the correlated sampling technique.[35] This technique takes advantage of the intermediate phase-space storage (IPSS) volume, a user-defined volume, which includes the positions of the detector along the profile, along the depth, or around the point of dose calculation. The simulation starts in the geometry outside the IPSS and stops in its surface where the particle phase space is stored. Then, this phase space is used for each position of the detector inside the IPSS. As the state of the number generator is also stored at the IPSS, there is maximum correlation between the calculated doses. The number of histories was chosen to obtain an statistical uncertainty of dose lower than 0.1% (1σ) for each (r,z) point.

2.B. Evaluation of perturbation correction factors

As described in the literature,[26,27] the dose in a small volume of water can be obtained from the response of a detector corrected by several correction factors that account for the non-water-like behavior of the several materials around the sensitive volume and that of the "cavity" itself, which are responsible for the dose perturbations. For the MC calculations, each perturbation factor is given by a ratio of doses scored in two different simulation geometries. Obtaining the absorbed dose in water requires that the product of all perturbation factors is equal to the ratio of the absorbed dose in water to the absorbed dose in the detector. To accomplish this goal, one defines different scoring volumes starting at the fully modeled detector and ending at a small volume of water placed at the reference point of the detector.[27] Using a procedure described previously,[27] we used MC simulations to calculate the following perturbation correction factors, as illustrated in Fig. 1:

(a) Microchamber: P_{stem}, P_{cel}, P_{wall}, $P_{\mathrm{fl}}(\bar{L}/\rho)_{\mathrm{si}}^{w}$, P_{ρ}, P_{geom}; these correction factors have been described in detail by Bouchard *et al.*[27]

(b) Diode: P_{wall1}, P_{wall2}, $P_{\mathrm{fl}}(\bar{L}/\rho)_{\mathrm{si}}^{w}$, P_{ρ}, P_{geom}.

(i) $P_{\mathrm{wall1}} = D_{\mathrm{wall2,si}}/D_{\mathrm{diode}}$, where D_{diode} is the absorbed dose in the sensitive layer of silicon in the fully modeled diode and $D_{\mathrm{wall2,si}}$ is the absorbed dose in the sensitive layer of silicon surrounded by only a substrate of silicon.

(ii) $P_{\mathrm{wall2}} = D_{\mathrm{si}}/D_{\mathrm{wall2,si}}$, where D_{si} is the absorbed dose in the bare sensitive layer of silicon.

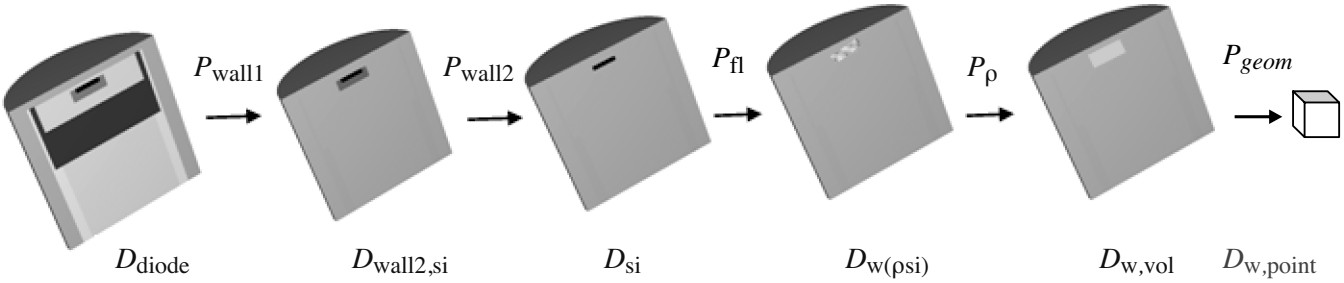

FIG. 1. Illustration of the series of cavity doses simulated to calculate the perturbation factors.

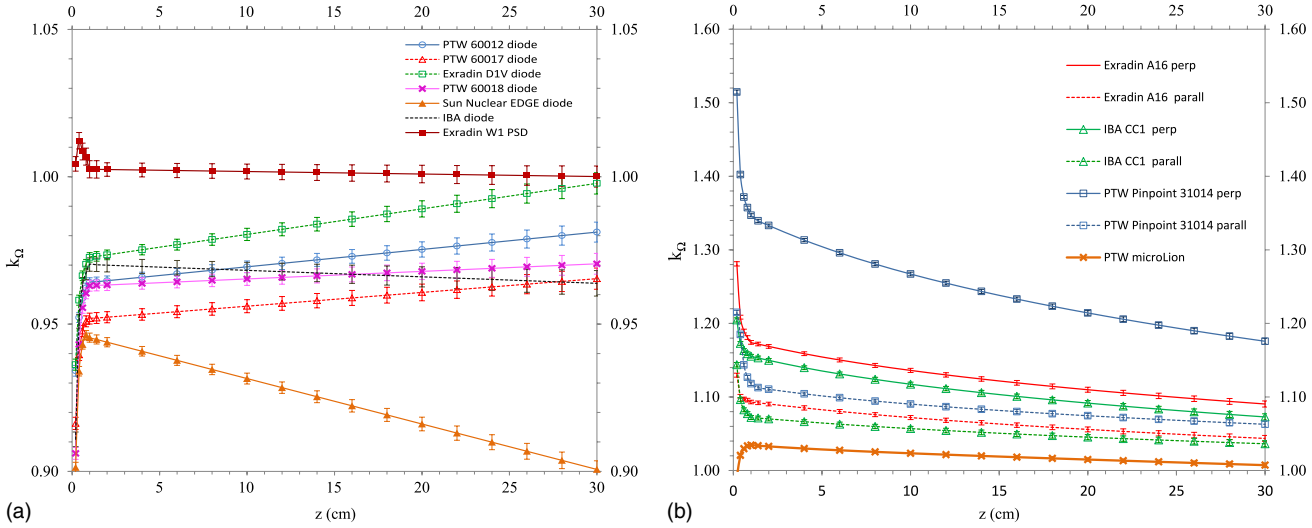

FIG. 2. Monte Carlo simulation of the variation of $k_\Omega(0, z, \mathrm{PDD})$ for (a) stereotactic diodes and the Exradin W1 PSD and (b) microchambers and the microLion, as a function of depth for a 5-mm circular collimator.

(iii) $P_{\mathrm{fl}}\left(\bar{L}/\rho\right)_{\mathrm{si}}^{w} = D_{w(\rho_{\mathrm{si}})}/D_{\mathrm{si}}$,
where $D_{w(\rho_{\mathrm{si}})}$ is the absorbed dose in the bare sensitive layer of silicon replaced with water with the same density as that of silicon (2.33 g/cm^3).

(iv) $P_\rho = D_{w,\mathrm{vol}}/D_{w(\rho\mathrm{si})}$,
where $D_{w,\mathrm{vol}}$ is the absorbed dose in the bare sensitive layer of silicon, replaced with water (density 1.0 g/cm^3).

(v) $P_{\mathrm{geom}} = D_{w,\mathrm{point}}/D_{w,\mathrm{vol}}$,
where $D_{w,\mathrm{point}}$ is the absorbed dose in a 0.5 $\times$0.5$\times$0.5 mm voxel of water placed at the reference point of the detector and represents the absorbed dose in water at the location of measurement.[27] This choice is justified because the dose clearly depends on the size of the scoring volume and one needs to define extremely small volumes to achieve the correct "point dose" result for better than 0.2% accuracy. This is not very practical, as it requires excessive computational time, and we believe that it will produce problems due to variability in scoring or voxel size (e.g., different groups using different point dose volumes). Given the above observations, we propose that dose be reported as an average dose in a volume of a given size. This will make it much easier to calculate correction factors and therefore limit error due to potentially different scoring volumes.

The perturbation correction factors (multiplying correction factors of the response of the detector) were used to demonstrate the actual effect or perturbation produced by the presence of the specific material studied as compared to the unperturbed situation (all waterlike materials).

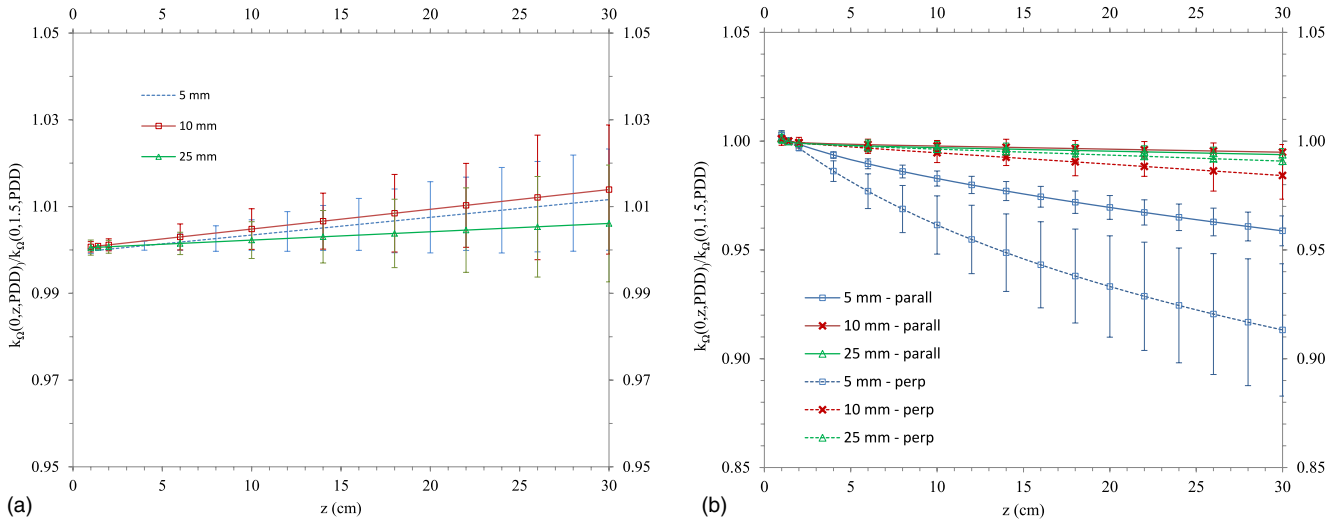

FIG. 3. The mean value of the $k_\Omega(0, z, \mathrm{PDD})$ for different collimator sizes of (a) all diodes, except the EDGE diode and (b) microchambers normalized at the value $k_\Omega(0, 1.5, \mathrm{PDD})$. Continuous line: stem axis parallel to the beam axis; dashed line: stem axis perpendicular to the beam axis.

To calculate the mean energy of photons and electrons at different depths, we used the FLURZnrc code without applying any variance reduction technique.

2.C. Experimental measurements

A PTW 60012 unshielded diode, a PTW 31014 PinPoint microchamber, and an Exradin W1 PSD were used to measure the OARs and PDDs of the 5- and 25-mm collimators of the CyberKnife system. The detectors were placed with their stems parallel to the beam axis, with the reference point of measurement corresponding to the depth of the active layer (i.e., 0.6 mm from the frontal surface for the PTW 60012 diode, 3.4 mm from the tip for the PTW 31014 PinPoint microchamber, and 2.26 mm from the frontal surface for the Exradin W1 PSD). Similar descriptions of this detectors setup are provided elsewhere.[17–19,37,38] For the OAR measurements, the source-to-surface distance was 70 cm, and the detectors were positioned with the reference point at a depth of 10 cm.

For the PDD measurements, the source-to-surface distance was 80 cm. The Exradin W1 PSD was chosen for its unique characteristics[37–40] as a countercheck of the accuracy of the MC simulations of the responses of different types of dosimeters. In fact, the Exradin W1 PSD is a fiber-based detector designed for the highly accurate measurement of small radiotherapy fields. This new near-water-equivalent PSD is manufactured by Standard Imaging, Inc. (Middleton, WI). The Exradin W1 PSD's sensitive element is composed of a plastic scintillating fiber enclosed inside a 2.8-mm diameter by 42-mm long water-equivalent robust housing probe. The dimensions of the plastic scintillating fiber are 1.0 mm in diameter and 3.0 mm in length. The density of the plastic scintillating fiber is 1.05 g/cm^3. The plastic scintillating fiber is coupled to a clear, 3-m-long multiclad optical fiber made of poly(methyl methacrylate) with a 1.0-mm-diameter core protected by a 2.2-mm-diameter polyethylene jacket. The scintillation light produced in the detector-sensitive element is transmitted through this 3-m optical fiber to a photodiode enclosed in a small, light-tight housing. The measurements were corrected for Cerenkov emission. The method for calibrating this detector for small-field measurement is different from the method described by the manufacturer, which applies to large-field measurements. In this case, the measurements were performed in water with the scintillator axis oriented parallel to the beam axis following the procedure described by Morin *et al.*[37] For the minimum exposed fiber condition, the optical fiber was pulled out of the field so that only about 10 cm of the fiber was within the beam without any significant optical bend; for the maximum exposed fiber condition, the optical fiber remained within the beam, extending to the bottom of the tank so that 25–30 cm of the optical fiber was irradiated. The fiber was not coiled in either condition. For both conditions, the effective point of measurement, which is the center of the scintillating fiber, was placed at the fixed reference depth of 1.5 cm, and a reference field size of 6-cm collimator.

The detectors were initially centered on the horizontal plane by means of using the crosshairs of the radiation field light. The detector position was finely tuned to within 0.1 mm to achieve the maximum signal intensity. Because a polarity effect has been observed with the microchamber,[10] measurements in the present study were averaged between positive and negative polarities (±400 V). The profiles were scanned with the diode and microchamber at 0.2-mm steps with a measuring time of 0.5 s/point and a speed of 50 mm/s. The PDDs were scanned at 1-mm steps in the buildup region and at 2-mm steps beyond buildup region. Because the Exradin W1 PSD does not lend itself to automatic water phantom scanning, the profiles and the PDDs were acquired using point-by-point measurements chosen manually. However, because the Exradin W1 PSD was used as a countercheck for each point, the measurements were repeated three times, and the mean of the three measurements was calculated.

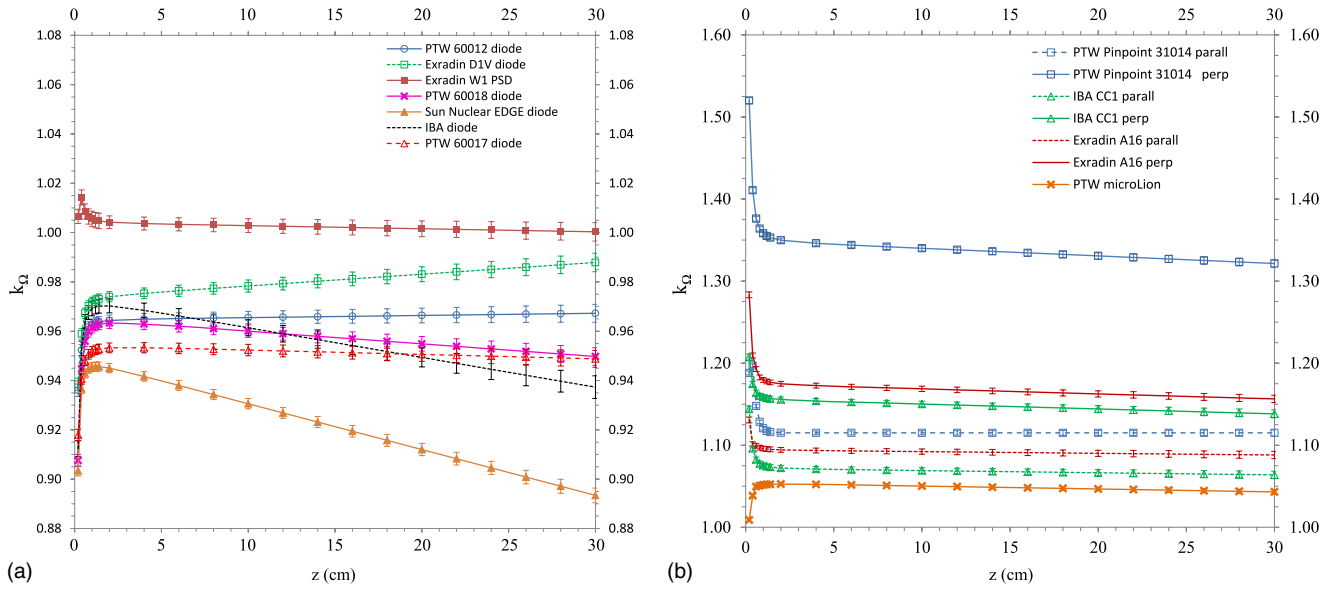

FIG. 4. Monte Carlo simulation of the variation of $k_\Omega(0, z, \mathrm{TMR})$ for (a) stereotactic diodes and the Exradin W1 PSD and (b) microchambers and the microLion, as a function of depth for a 5-mm circular collimator on a CyberKnife system in parallel and perpendicular stem orientations.

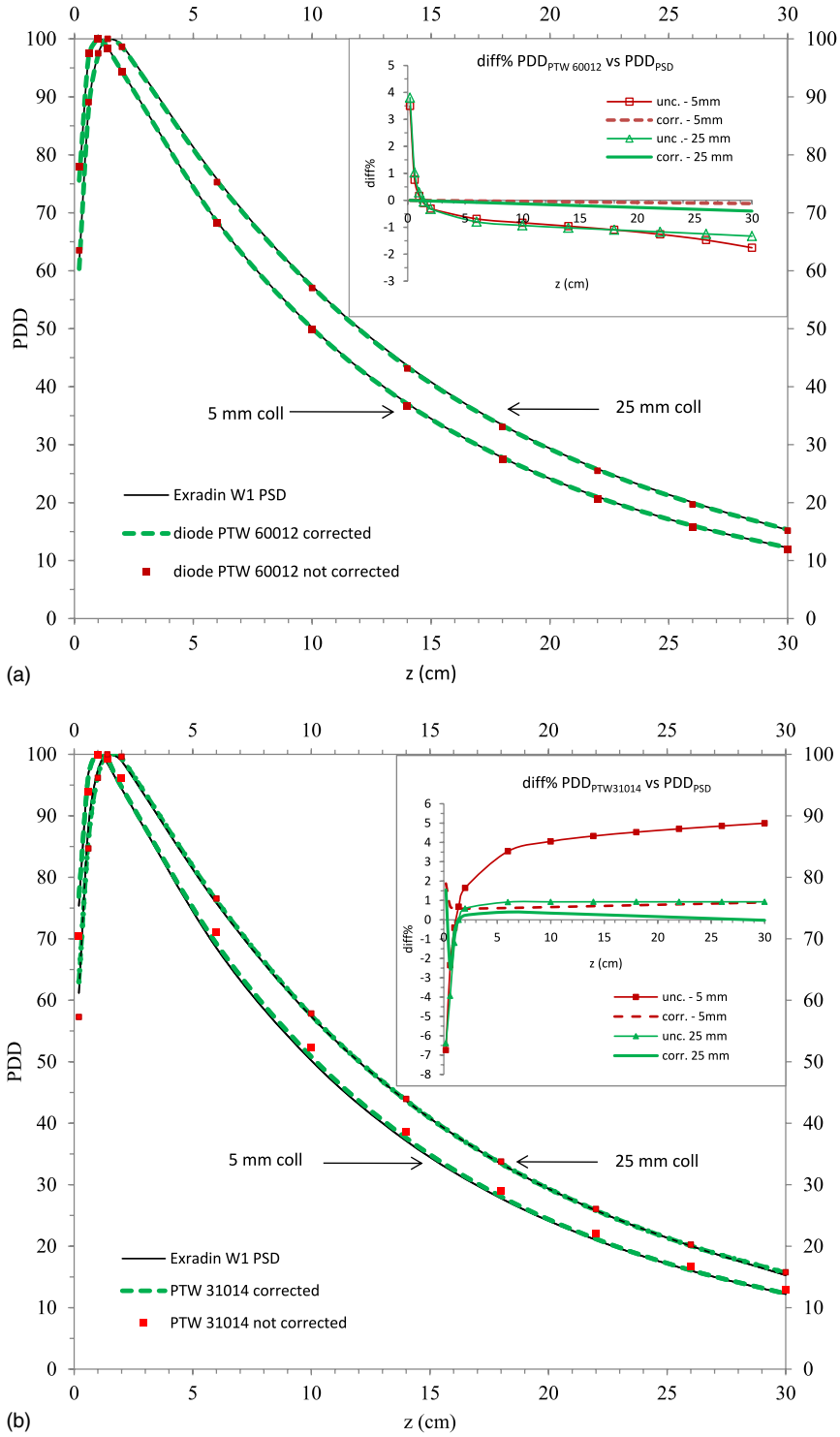

FIG. 5. PDD of the 5- and 25-mm collimators measured with (a) the Exradin W1 PSD and the diode PTW 60012 and (b) the Exradin W1 PSD and the PTW 31014 microchamber with the stem axis parallel to the beam axis before and after applying the correction factor k_{Ω}. The difference plot is also magnified to show the extent of difference (inset).

2.D. Experimental uncertainties

The PDD and OAR experimental uncertainties were estimated in the following ways. The uncertainty of the dose at each point due to the uncertainty in the accuracy with which the machine isocenter location is known and the detector is positioned were calculated using the code developed by Bouchard *et al.*[41] The code estimates the uncertainty in dose measurements due to setup positioning errors of the detector and isocenter of the machine by simulating N different positions of the entire system (including the position of the source and the system of measurement) and repeating M simulations for each position. It then repeats the entire simulation for K samples (a sample corresponds to $M \times N$ number of histories),

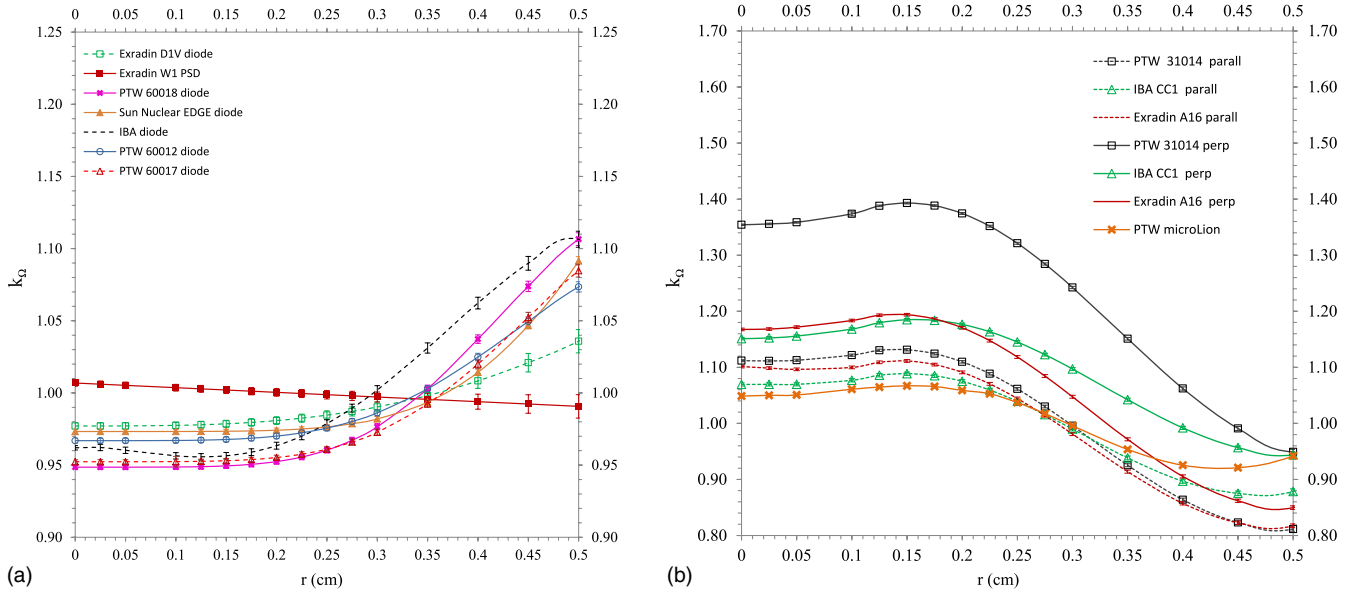

FIG. 6. Monte Carlo simulation of the variation of $k_\Omega(r, 10, \mathrm{OAR})$ as a function of distance from the central axis for a 5-mm circular collimator for (a) the stereotactic diodes and the Exradin W1 PSD and (b) the microchambers.

with each sample having the same meaning of a different session of measurements. In this code, two different types of probability distributions have been implemented to describe the displacement of the detector and/or isocenter during the simulations: (1) a uniform distribution that is delimitated by a maximum shift and (2) a Gaussian distribution defined by a standard deviation value and limited by a maximum shift. In calculating the positioning-induced dose uncertainty, we made the following assumptions: the position of the isocenter had an uncertainty of 0.1 mm in the x and y direction and 1 mm in the z direction; the uncertainty of the rotation angle in the z direction of the isocenter was 0.1°; and the position uncertainty of the dosimeter was 0.1 mm in the x, y, and z directions. In both cases, a uniform statistical distribution was assumed. For the geometrical uncertainty, the uncertainties due to fluctuations in the response of the dosimeter were summed in quadrature to obtain the total uncertainty that was used for plotting the data.

3. RESULTS

In general, these data are divided into two groups, with data for the solid-state detectors, diodes, and scintillator shown in (a) and those for microchambers shown in (b) in each figure. This separation was performed to illustrate the difference between ion chamber and other detectors. Figures 2(a) and 2(b) show the variation of $k_\Omega(0,z,\mathrm{PDD})$ for the 5-mm collimator defined at 80 cm from the source for the stereotactic diodes, Exradin W1 PSD, microchambers, and microLion.

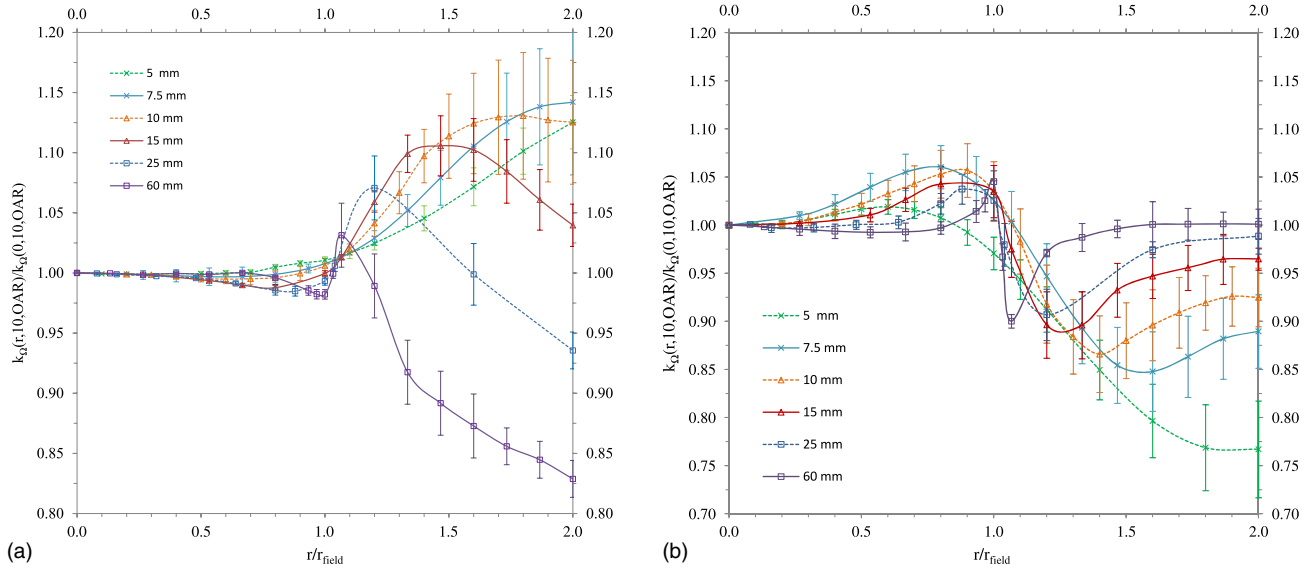

FIG. 7. The mean $k_\Omega(r, 10, \mathrm{OAR})$ for all diodes, except the EDGE diode (a) and all microchambers (b) for different field dimensions as a function of the ratio r/r_{field} normalized at the value of $k_\Omega(0, 10, \mathrm{OAR})$.

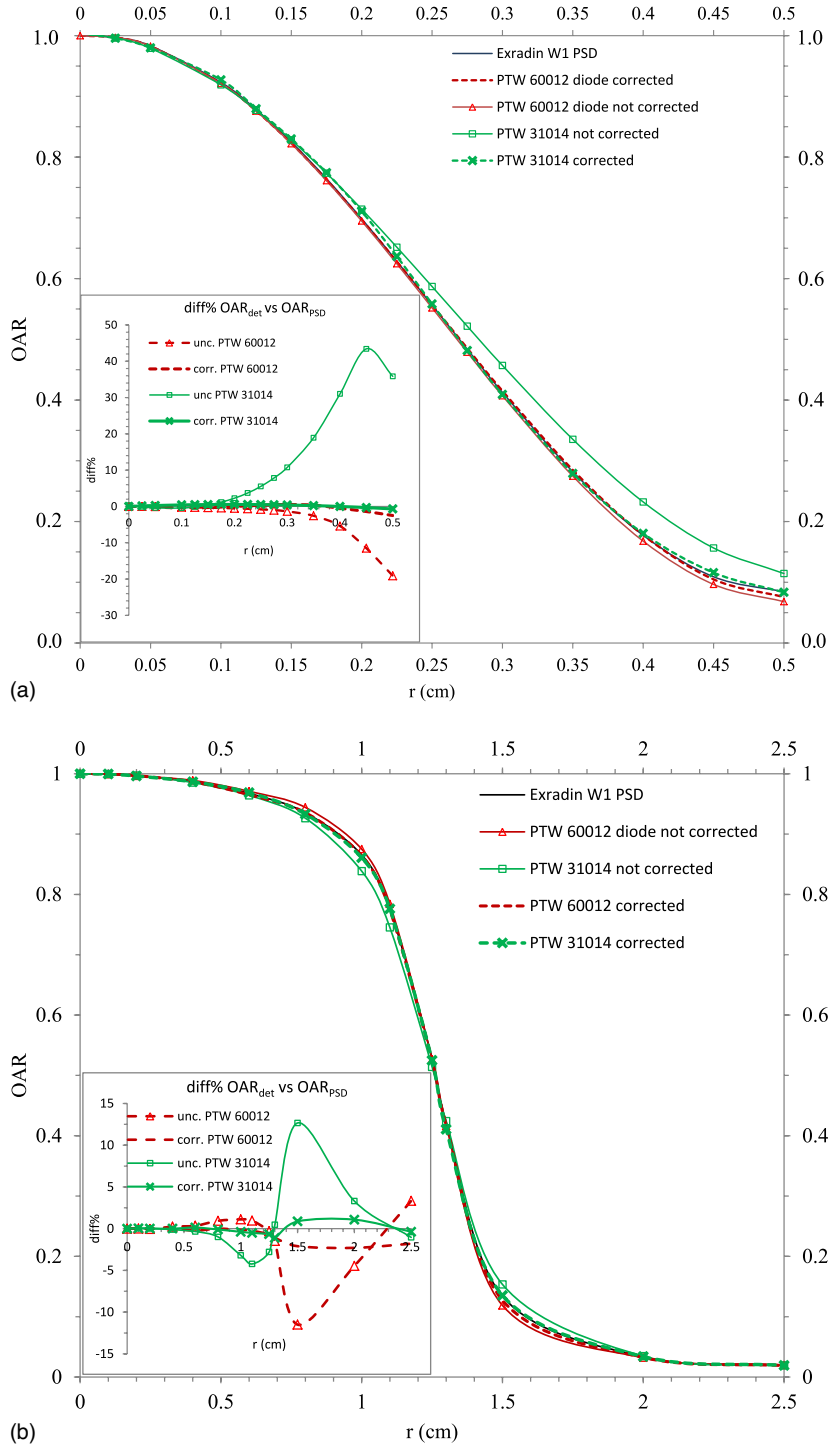

FIG. 8. OAR of the 5-mm collimator measured at a depth of 10 cm with the scintillator detector, PTW 60012 diode, and PTW 31014 microchamber with the stem axis parallel to the beam axis before and after applying the correction factor k_Ω for (a) the 5-mm collimator and (b) the 25-mm collimator. The difference plot is also magnified to show the extent of difference (inset).

Figures 3(a) and 3(b) show the mean $k_\Omega(0,z,\text{PDD})$ values of all diodes, except the EDGE diode, and those of all microchambers for different field diameters normalized to the mean $k_\Omega(0,1.5,\text{PDD})$ value.

Figure 4 shows the variation in $k_\Omega(0,z,\text{TMR})$ as a function of depth for the 5-mm collimator with the stereotactic diodes and the Exradin W1 PSD. Data for the microchambers and microLion in parallel and perpendicular stem orientations are also shown.

The experimental results for the PDD measurements for various detectors (the PTW 60012 diode and PTW PinPoint 31014 microchamber) and the Exradin W1 PSD for the 5- and 25-mm diameter cones are shown in Fig. 5. The MC k_Ω were used to correct readings for PDD. Because the PDD lines

TABLE I. The perturbation factors of the dose response for the PDD geometry as discussed in Sec. 2.B for (a) the PTW 60012 diode, (b) the Sun Nuclear EDGE diode, and (c) the PTW PinPoint 31014 microchamber with respect to water of 5- and 25-mm collimators as a function of depth. The PinPoint microchamber was simulated with the stem axis perpendicular to the beam axis.

(a) PTW 60012 diode

Depth	P_{wall1}		P_{wall2}		$P_{fl}(L/\rho)^w_{Si}$		P_ρ		P_{geom}		$D_{w,point}/D_{diode}$	
(cm)	5 mm	25 mm	5 mm	25 mm	5 mm	25 mm	5 mm	25 mm	5 mm	25 mm	5 mm	25 mm
0.2	0.956	0.960	0.876	0.892	1.205	1.205	0.993	0.996	1.000	1.000	1.002	1.030
0.5	0.963	0.973	0.883	0.901	1.209	1.211	0.995	1.000	1.006	1.001	1.029	1.063
1.5	0.962	0.977	0.889	0.908	1.210	1.214	0.994	0.999	1.006	1.002	1.035	1.077
10	0.957	0.975	0.894	0.914	1.215	1.216	0.996	0.999	1.003	1.000	1.039	1.082
30	0.950	0.970	0.910	0.923	1.219	1.219	0.995	0.999	1.005	1.001	1.053	1.094

(b) Sun Nuclear EDGE diode

Depth	P_{wall1}		P_{wall2}		$P_{fl}(L/\rho)^w_{Si}$		P_ρ		P_{geom}		$D_{w,point}/D_{diode}$	
(cm)	5 mm	25 mm	5 mm	25 mm	5 mm	25 mm	5 mm	25 mm	5 mm	25 mm	5 mm	25 mm
0.2	0.797	0.786	0.905	0.918	1.212	1.213	0.988	0.999	1.001	1.002	0.865	0.874
0.5	0.814	0.819	0.919	0.937	1.216	1.217	0.991	1.000	1.004	1.000	0.905	0.934
1.5	0.812	0.833	0.924	0.945	1.216	1.220	0.997	0.999	1.004	1.000	0.913	0.960
10	0.794	0.825	0.926	0.949	1.221	1.220	0.997	0.999	1.004	1.000	0.899	0.954
30	0.763	0.806	0.938	0.957	1.223	1.222	0.996	0.999	1.004	1.000	0.875	0.939

(c) PTW PinPoint 31014 microchamber (perp)

Depth	P_{stem}		P_{cel}		P_{wall}		$P_{fl}(L/\rho)^w_{air}$		P_ρ		P_{geom}		$D_{w,point}/D_{PinPoint}$	
(cm)	5 mm	25 mm	5 mm	25 mm	5 mm	25 mm	5 mm	25 mm	5 mm	25 mm	5 mm	25 mm	5 mm	25 mm
0.2	1.034	1.013	0.979	0.989	0.947	0.968	1.125	1.127	1.300	1.128	1.227	1.010	1.720	1.244
0.5	1.029	1.009	0.984	0.995	0.975	0.991	1.121	1.123	1.172	1.031	1.208	1.000	1.567	1.150
1.5	1.025	1.010	0.989	0.996	0.979	1.000	1.117	1.119	1.143	1.003	1.193	1.001	1.512	1.129
10	1.023	1.010	0.990	0.996	0.981	1.001	1.115	1.117	1.122	1.000	1.151	1.002	1.431	1.127
30	1.018	1.008	0.993	0.997	0.985	1.001	1.109	1.113	1.090	0.999	1.097	0.999	1.320	1.119

are not discernible, the percentage differences before and after applying the correction factor k_Ω are plotted (inset). The experimental comparison percentage difference between the PDDs obtained with the PTW 60012 diode and the PTW PinPoint 31014 microchamber vs the PDDs obtained with the Exradin W1 PSD are clearly visible [Figs. 5(a) and 5(b)].

The OAR dependence is shown in Figs. 6(a) and 6(b) indicating the variation of $k_\Omega(r,10,OAR)$ for the stereotactic diodes, Exradin W1 PSD, and various microchambers.

The mean $k_\Omega(r,10,OAR)$ of all diodes, except the EDGE diode, and that of all microchambers for different field diameters normalized at the $k_\Omega(0,10,OAR)$ value are shown in Figs. 7(a) and 7(b).

Finally, the impact of k_Ω on OAR measured using various detectors for 5- and 25-mm diameter cones are shown in Figs. 8(a) and 8(b). Also shown are the experimental percentage differences between the OARs obtained with the PTW 60012 diode and the PTW PinPoint 31014 microchamber vs the OARs obtained with the Exradin W1 PSD before and after applying the correction factor k_Ω (inset).

Table I shows the factorization of the response of the PTW 60012 diode, the Sun Nuclear EDGE diode, and the PTW PinPoint 31014 microchamber with respect to water of 5- and 25-mm collimators as a function of the depth for the PDD geometry.

Table II shows the factorization of the response of the PTW 60012 diode, the Sun Nuclear EDGE diode, and the PTW PinPoint 31014 microchamber with respect to water of 5- and 25-mm collimators as a function of the depth for the TMR geometry.

Table III shows the factorization of the response of the PTW 60012 diode, the Sun Nuclear EDGE diode, and the PinPoint 31014 microchamber with respect to water of 5- and 25-mm collimators as a function of the distance from the central axis at a depth of 10 cm.

Table IV shows the change in the mean energy of electrons and photons as the depth increases for the 5-mm collimator.

Table V shows the change in the mean energy of electrons and photons as the distance from the central axis increases for three different collimators.

3.A. Experimental uncertainties in PDD measurements

The uncertainty due to detector positioning and the uncertainty due to the fluctuations in the response of the dosimeter were about 0.24% and 0.1%, respectively, that summed in quadrature give the value of 0.26%. Figure 9(a) shows how the uncertainty for the 5-mm collimator changed as a function

TABLE II. The perturbation factors of the dose response for the TMR geometry for (a) the PTW 60012 diode, (b) the Sun Nuclear EDGE diode, and (c) the PTW PinPoint 31014 microchamber with respect to water for 5- and 25-mm collimators as a function of depth. The PinPoint microchamber was simulated with the stem axis perpendicular to the beam axis.

(a) PTW 60012 diode

Depth	P_{wall1}		P_{wall2}		$P_{fl}(L/\rho)^{w}_{Si}$		P_{ρ}		P_{geom}		$D_{w,point}/D_{diode}$	
(cm)	5 mm	25 mm	5 mm	25 mm	5 mm	25 mm	5 mm	25 mm	5 mm	25 mm	5 mm	25 mm
0.2	0.956	0.960	0.877	0.893	1.201	1.205	0.994	0.996	1.005	1.000	1.006	1.027
0.5	0.963	0.973	0.884	0.902	1.207	1.212	0.995	0.999	1.007	0.998	1.030	1.060
1.5	0.963	0.977	0.889	0.909	1.207	1.213	0.996	1.000	1.005	1.000	1.034	1.076
10	0.957	0.976	0.892	0.913	1.213	1.215	0.995	1.000	1.007	1.000	1.037	1.083
30	0.947	0.970	0.906	0.924	1.216	1.220	0.996	0.999	1.008	1.000	1.047	1.092

(b) Sun Nuclear EDGE diode

Depth	P_{wall1}		P_{wall2}		$P_{fl}(L/\rho)^{w}_{Si}$		P_{ρ}		P_{geom}		$D_{w,point}/D_{diode}$	
(cm)	5 mm	25 mm	5 mm	25 mm	5 mm	25 mm	5 mm	25 mm	5 mm	25 mm	5 mm	25 mm
0.2	0.797	0.786	0.905	0.917	1.213	1.214	0.995	0.998	1.004	1.000	0.870	0.873
0.5	0.813	0.817	0.919	0.935	1.214	1.218	0.997	0.999	1.004	1.002	0.904	0.933
1.5	0.812	0.833	0.923	0.945	1.216	1.220	0.996	0.999	1.004	1.000	0.915	0.959
10	0.796	0.824	0.923	0.948	1.221	1.222	0.996	1.000	1.004	1.002	0.897	0.954
30	0.766	0.804	0.926	0.952	1.223	1.225	0.994	0.999	1.005	1.002	0.867	0.936

(c) PTW PinPoint 31014 microchamber (perp)

Depth	P_{stem}		P_{cel}		P_{wall}		$P_{fl}(L/\rho)^{w}_{air}$		P_{ρ}		P_{geom}		$D_{w,point}/D_{PinPoint}$	
(cm)	5 mm	25 mm	5 mm	25 mm	5 mm	25 mm	5 mm	25 mm	5 mm	25 mm	5 mm	25 mm	5 mm	25 mm
0.2	1.034	1.012	0.979	0.989	0.947	0.968	1.124	1.126	1.301	1.129	1.227	1.008	1.721	1.241
0.5	1.030	1.010	0.985	0.994	0.973	0.993	1.120	1.122	1.175	1.032	1.213	1.002	1.577	1.154
1.5	1.025	1.009	0.987	0.996	0.979	1.001	1.118	1.118	1.147	1.003	1.200	1.002	1.525	1.129
10	1.023	1.009	0.989	0.996	0.978	1.001	1.114	1.117	1.149	1.001	1.195	1.002	1.514	1.127
30	1.021	1.009	0.989	0.997	0.976	1.001	1.108	1.112	1.150	1.001	1.187	1.003	1.493	1.126

of the uncertainty in the detector positioning in the x, y, and z axes for PDDs for various detectors.

3.B. Experimental OAR uncertainties

The uncertainty in dosimeter position influences the uncertainty of the OAR value differently depending on the dosimeter's distance from the central axis and has a maximum where the dose gradient is maximum. The variation of the OAR uncertainty as a function of the distance of the detector from the central axis is shown in Fig. 9(b). Different values of the uncertainty in the detector positioning along the x, y, and z axes were considered. For our setup, an uncertainty of 0.1 mm was assumed.

4. DISCUSSION

The stereotactic diodes, except the Sun Nuclear EDGE diode, which has a layer of copper below the sensitive volume, reproduced the PDD and TMR in water to within 2% at all depths beyond the buildup region [Figs. 2(a) and 4(a)]. The data in Tables I(a), I(b), II(a) and II(b) provide some insight into the changes of PDD and TMR with detectors. Near the surface (i.e., at a depth of 0.2 cm), the diodes exhibit an electron fluence perturbation (EFP) in the sensitive volume due to the materials around the sensitive volume and atomic composition of the silicon of the sensitive volume.

The density of the sensitive volume's material (2.33 g/cm^3) and the geometrical factor have an insignificant influence on EFP. As the depth increases, the EFP due to the materials around the sensitive volume (except the silicon of the chip) decreases (P_{wall1} increases and tends to 1) in the buildup region and then increases (P_{wall1} decreases); the EFP due to the silicon of the chip around the sensitive volume decreases monotonically with depth (P_{wall2} increases). The EFP due to the materials around the sensitive volume except the silicon of the chip is greater for the EDGE diode than for the other diodes owing to its dimensions (a parallelepiped of $3.8 \times 0.55 \times 0.38$ cm) and to its materials composition (brass housing, a layer of copper below the sensitive volume, etc.). Figure 3(a) shows that as the collimator diameter increases, the change of the mean response of all diodes (except the EDGE diode) with depth decreases, although very little. Tables I(a) and I(b) show that as the collimator diameter increases from 5- to 25-mm, the EFP due to the materials around the sensitive volume decreases (P_{wall1} and P_{wall2} tend to 1), and its relative change as a function of depth from 1.5 to 30 cm is almost the same for the PTW 60012 diode ($P_{wall1} \cdot P_{wall2} = +0.9\%$ for the 5-mm collimator vs $P_{wall1} \cdot P_{wall2} = +0.8\%$ for the 25-mm collimator) but significantly smaller for the

TABLE III. The perturbation factors of the dose response as used in OAR for (a) the PTW 60012 diode, (b) the Sun Nuclear EDGE diode, and (c) the PTW PinPoint 31014 microchamber with respect to water of 5- and 25-mm collimators as a function of the distance from the central axis. The correction factors were calculated at a depth of 10 cm with a source-to-surface distance of 70 cm. The PinPoint microchamber was simulated with the stem axis perpendicular to the beam axis.

(a) PTW 60012 diode

	P_{wall1}		P_{wall2}		$P_{fl}(L/\rho)^w_{Si}$		P_ρ		P_{geom}		$D_{w,point}/D_{diode}$	
r/r_{field}	5 mm	25 mm	5 mm	25 mm	5 mm	25 mm	5 mm	25 mm	5 mm	25 mm	5 mm	25 mm
0.0	0.957	0.976	0.893	0.913	1.213	1.215	0.994	1.000	1.007	1.000	1.037	1.083
0.6	0.957	0.971	0.893	0.911	1.213	1.216	0.996	0.998	1.006	1.000	1.039	1.074
1.0	0.961	0.975	0.900	0.911	1.215	1.214	0.995	0.999	1.005	1.003	1.051	1.078
1.4	0.966	1.025	0.916	0.935	1.218	1.187	1.001	1.002	0.995	1.000	1.079	1.140
2.0	0.995	0.988	0.951	0.907	1.224	1.126	1.009	0.996	0.989	1.005	1.156	1.006

(b) Sun Nuclear EDGE diode

	P_{wall1}		P_{wall2}		$P_{fl}(L/\rho)^w_{Si}$		P_ρ		P_{geom}		$D_{w,point}/D_{diode}$	
r/r_{field}	5 mm	25 mm	5 mm	25 mm	5 mm	25 mm	5 mm	25 mm	5 mm	25 mm	5 mm	25 mm
0.0	0.796	0.824	0.923	0.948	1.221	1.222	0.996	1.000	1.004	1.002	0.897	0.954
0.6	0.800	0.817	0.923	0.945	1.221	1.223	0.995	0.998	1.006	1.000	0.897	0.942
1.0	0.798	0.828	0.933	0.945	1.221	1.217	0.996	1.000	1.004	1.005	0.906	0.953
1.4	0.796	1.007	0.956	0.963	1.224	1.193	1.002	1.008	0.995	0.993	0.929	1.167
2.0	0.864	0.959	0.994	0.919	1.233	1.137	1.006	1.004	0.991	0.999	1.056	1.006

(c) PTW PinPoint 31014 microchamber (perp)

	P_{stem}		P_{cel}		P_{wall}		$P_{fl}(L/\rho)^w_{air}$		P_ρ		P_{geom}		$D_{w,point}/D_{PinPoint}$	
r/r_{field}	5 mm	25 mm	5 mm	25 mm	5 mm	25 mm	5 mm	25 mm	5 mm	25 mm	5 mm	25 mm	5 mm	25 mm
0.0	1.023	1.009	0.989	0.996	0.978	1.001	1.114	1.117	1.149	1.001	1.195	1.002	1.514	1.127
0.6	1.022	1.009	0.988	0.996	0.981	0.999	1.114	1.116	1.140	1.008	1.235	1.006	1.554	1.138
1.0	1.019	1.013	0.991	0.995	0.990	1.001	1.116	1.116	1.082	1.015	1.228	1.041	1.481	1.191
1.4	1.016	1.008	0.998	0.996	1.008	1.020	1.115	1.124	0.977	0.938	1.149	1.001	1.279	1.080
2.0	1.014	1.008	1.001	0.990	1.018	1.007	1.117	1.129	0.927	0.991	1.099	1.003	1.176	1.128

EDGE diode ($P_{wall1} \cdot P_{wall2} = -3.9\%$ for the 5-mm collimator vs $P_{wall1} \cdot P_{wall2} = -1.8\%$ for the 25-mm collimator).

The microchambers [Fig. 2(b)] show for the PDDs a response that increases as the depth increases. This effect is greater if the stem axis is perpendicular to the beam axis because in this case the area occupied by the chamber on the plane perpendicular to the beam axis is greater. This behavior mainly depends on the EFP due to the presence of a material of very low density (air) in the cavity and on the dimensions of the chamber compared to the varying field dimensions with depth [P_ρ and P_{geom}, respectively, in Table I(c)]. In the buildup region, the field dimensions increase very little; therefore, the geometrical factor P_{geom} changes much less than P_ρ does. The other factors change relatively little, and their variation depends on the increase of the mean energy of photons and electrons with depth (Table IV). Figure 3(b) shows that as the collimator diameter increases, there is a significant decrease in the change of k_Ω with depth. Table I(c) shows that this behavior depends mainly on the density and the geometrical factors P_ρ and P_{geom}. Therefore, the microchambers can be used for PDD measurements for collimators greater than 10 mm in diameter without applying a correction factor.

The values of $k_\Omega(0,z,\text{PDD})$ are indirectly confirmed by the data in Figs. 5(a) and 5(b), which show that after applying the

TABLE IV. Change in the mean energy of electrons and photons in water as depth increases for the 5-mm collimator. The PDD geometry was used.

Depth (cm)	Mean electron energy (MeV)	Mean photon energy (MeV)
0.2	0.838	1.496
1.5	1.059	1.532
10	1.156	1.833
30	1.351	2.483

TABLE V. Change in the mean energy of electrons and photons off-axis from the central axis in water.

r/r_{field}	Collimator (mm)	Mean electron energy (MeV)	Mean photon energy (MeV)
0	5	1.156	1.833
0	25	1.099	1.688
0	60	1.064	1.476
2	5	1.043	1.380
2	25	0.642	0.551
2	60	0.364	0.325

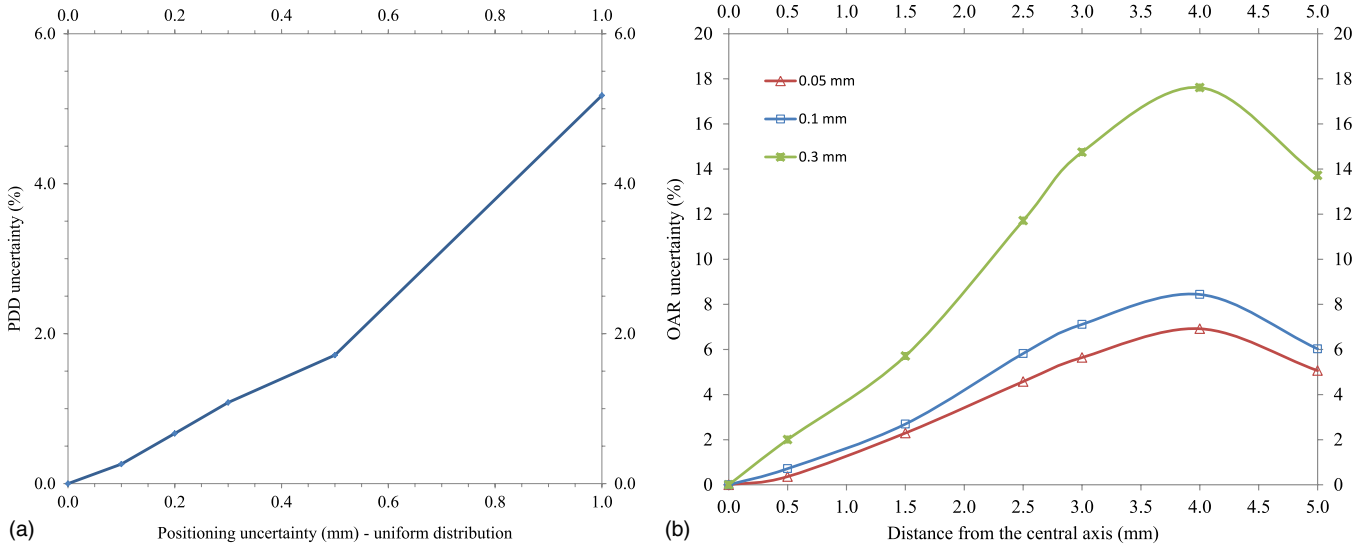

FIG. 9. Uncertainties in PDD (a) and OAR (b) for the 5-mm collimator as a function of positioning uncertainty of the detector in the x, y, and z axes, assuming a uniform distribution.

$k_\Omega(0,z,\text{PDD})$ correction factor, the experimental PDDs obtained with the PTW 60012 diode, the PTW PinPoint 31014 microchamber, and the Exradin W1 PSD coincide within the experimental uncertainty both for the 5- and 25-mm collimators.

In the TMR measurements, by definition, the field size remains constant for every depth and thus k_Ω remains unchanged related to the change of field dimensions. This is reflected in Fig. 4(b). Therefore, even the microchambers can be used without applying a correction factor for measurements of TMR for all the collimators as long as the detector is comparatively small.

Figure 6 shows that neither the stereotactic diodes nor the microchambers correctly reproduce the dose profiles in water. Only the Exradin W1 PSD can be considered water-equivalent and is suitable for the measurement. Unfortunately, this detector requires point-by-point measurement and cannot be used as a scanning detector.

The values of $k_\Omega(r,10,\text{OAR})$ are indirectly confirmed by the data in Figs. 8(a) and 8(b), which show that after applying the $k_\Omega(r,10,\text{OAR})$ correction factor, the experimental OARs obtained with the PTW 60012 diode, the PTW PinPoint 31014 microchamber, and the Exradin W1 PSD coincide within the experimental uncertainty both for the 5 and 25 mm collimators.

For the 5-mm collimator, the diodes reproduce with an acceptable accuracy the OAR in water up to the penumbra region [Fig. 6(a)]; in the tail regions, the diodes significantly underestimate the OAR in water (k_Ω increases). Tables III(a) and III(b) show that this behavior depends on complex changes in P_{wall1} and P_{wall2} as the distance from the central axis increases. As the collimator diameter increases [Fig. 7(a)], the relative response of the diodes increases in the tail region; from the 25-mm collimator, there is an overestimation of the OAR in water in this region (k_Ω decreases). For larger fields [Tables III(a) and III(b)], the change in P_{fl} becomes significant owing to the decrease in the mean energy of photons and electrons in the tail region (Table V). The same pattern has also been shown by Verhaegen *et al.*[42]

For the 5 mm collimator, the microchambers overestimate the OAR in water (k_Ω decreases) in the penumbra region; in the tail region, the overestimation is almost constant [Fig. 7(b)]. As the collimator diameter increases, the overestimation decreases. Table III(c) shows that for the microchamber, the most important factor is the change in EFP due to the very small density (air) contained in the cavity P_ρ as the distance increases from the central axis. However, the volume effect P_{geom} that is generally considered the most important factor has relatively less influence.

5. CONCLUSIONS

We have provided k_Ω values for various microdetectors in the context of PDD, TMR, and OAR in small fields. We conclude that the Exradin W1 PSD is the only detector that can reproduce the PDD and OAR in water with remarkable accuracy compared to the MC simulation data. However, it is not possible to use this dosimeter for scanning data measurements of OAR and PDD; therefore, its use in clinical practice remains difficult until the manufacturer makes such a detector available for scanning. In the future, near-water-equivalent dosimeters, such as those fabricated with synthetic microdiamond, could be used with minimum correction.[23] Another best choice is to utilize a stereotactic diode that achieves PDDs that mimic those in water with a systematic error of less than 2%. The stereotactic diode correctly reproduced the OAR in water up to the penumbra zone but significantly underestimated the value of OAR in the tail region. One could argue that this systematic error has little clinical importance, as it is associated with a region of very low dose. However, the facts that CyberKnife treatments use many fields and that the low isodoses occupy relative large volumes should prompt one to reflect carefully on the possible underestimation of the long-term effects.

More important, the results of this study suggest that microchambers should not be used for OAR measurements of small fields.

MC simulations provide suitable data where measurements cannot be performed. It is concluded that detectors that are water-equivalent and small compared to the resolution of required data may be ideally suited with minimal perturbation in small fields.

ACKNOWLEDGMENT

Sam Beddar would like to acknowledge partial support from a National Cancer Institute Grant (2R44CA153824-02A1) entitled "Water-Equivalent Plastic Scintillation Detectors for Small Field Radiotherapy-Phase II."

[a]Author to whom correspondence should be addressed. Electronic mail: paolo.francescon@ulssvicenza.it

[1]*Radiation Oncology Physics: A Handbook for Teachers and Students*, edited by Podgorsak (International Atomic Energy Agengy, Vienna, 2005).
[2]I. J. Das, C. W. Cheng, R. J. Watts, A. Ahnesjö, J. Gibbons, X. A. Li, J. Lowenstein, R. K. Mitra, W. E. Simon, and T. C. Zhu, "Accelerator beam data commissioning equipment and procedures: Report of the TG-106 of the Therapy Physics Committee of the AAPM," Med. Phys. **35**, 4186–4215 (2008).
[3]P. Alfonso, P. Andreo, R. Capote, M. S. Huq, W. Kilby, P. Kjall, T. R. Mackie, H. Palmans, K. Rosser, J. Seuntjens, W. Ullrich, and S. Vatnitsky, "A new formalism for reference dosimetry of small and nonstandard fields," Med. Phys. **35**, 5179–5186 (2008).
[4]M. M. Aspradakis, "Small field MV dosimetry," Report No. 103 (IPEM, York, England, 2010).
[5]I. J. Das, P. Francescon, A. Ahnesjö, M. M. Aspradakis, C. W. Cheng, G. X. Ding, J. Fenwick, G. S. Ibbott, M. Oldham, M. S. Huq, C. S. Reft, and O. A. Sauer, "Small fields and non-equilibrium condition photon beam dosimetry: AAPM Task Group Report 155," Med. Phys. (2014) (in review).
[6]I. J. Das, G. X. Ding, and A. Ahnesjö, "Small fields: Non-equilibrium radiation dosimetry," Med. Phys. **35**, 206–215 (2008).
[7]I. J. Das, M. B. Downes, A. Kassaee, and Z. Tochner, "Choice of radiation detector in dosimetry of stereotactic radiosurgery-radiotherapy," J. Radiosurg. **3**, 177–185 (2000).
[8]T. C. Zhu, B. E. Bjarngard, and H. Shackford, "X-ray source and the output factor," Med. Phys. **22**, 793–798 (1995).
[9]A. Wu, R. D. Zwicker, A. M. Kalend, and Z. Zheng, "Comments on dose measurements for a narrow beam in radiosurgery," Med. Phys. **20**, 777–779 (1993).
[10]K. De Vlamynck, H. Palmans, F. Verhaegen, C. De Wagter, W. De Neve, and H. Thierens, "Dose measurements compared with Monte Carlo simulations of narrow 6 MV multileaf collimator shaped photon beams," Med. Phys. **26**, 1874–1882 (1999).
[11]F. Araki, "Monte Carlo study of a CyberKnife stereotactic radiosurgery system," Med. Phys. **33**, 2955–2963 (2006).
[12]R. K. Rice, J. L. Hansen, G. K. Svensson, and R. L. Siddon, "Measurements of dose distributions in small beams of 6 MV x-rays," Phys. Med. Biol. **32**, 1087–1099 (1987).
[13]P. Francescon, S. Cora, C. Cavedon, P. Scalchi, S. Reccanello, and F. Colombo, "Use of a new type of radiochromic film, a new parallel-plate micro-chamber, MOSFETs, and TLD 800 microcubes in the dosimetry of small beams," Med. Phys. **25**, 503–511 (1998).
[14]R. Capote, F. Sanchez-Doblado, A. Leal, J. I. Lagares, R. Arrans, and G. H. Hartmann, "An EGSnrc Monte Carlo study of the microionization chamber for reference dosimetry of narrow irregular IMRT beamlets," Med. Phys. **31**, 2416–2422 (2004).
[15]H.-R. Lee, M. Pankuch, and J. Chu, "Evaluation and characterization of parallel plate microchamber's functionalities in small beam dosimetry," Med. Phys. **29**, 2489–2496 (2002).
[16]C. McKerracher and D. I. Thwaites, "Assessment of new small-field detectors against standard-field detectors for practical stereotactic beam data acquisition," Phys. Med. Biol. **44**, 2143–2160 (1999).
[17]P. Francescon, S. Cora, and N. Satariano, "Calculation of k(Q(clin),Q(msr)) (f(clin),f(msr)) for several small detectors and for two linear accelerators using Monte Carlo simulations," Med. Phys. **38**, 6513–6527 (2011).
[18]P. Francescon, W. Kilby, N. Satariano, and S. Cora, "Monte Carlo simulated correction factors for machines specific reference field dose calibration and output factor measurement using fixed and iris collimators on the CyberKnife system," Phys. Med. Biol. **57**, 3741–3258 (2012).
[19]P. Francescon, W. Kilby, and N. Satariano, "Monte Carlo simulated correction factors or output factor measurement with the CyberKnife system—Results for new detectors and correction factor dependence on measurement distance and detector orientation," Phys. Med. Biol. **59**, N11–N17 (2014).
[20]G. Cranmer-Sargison, S. Weston, N. P. Sidhu, and D. I. Thwaites, "Experimental small field 6 MV output ratio analysis for various diode detector and accelerator combinations," Radiother. Oncol. **24**, 429–435 (2011).
[21]D. Czarnecki and K. Zink, "Monte Carlo calculated correction factors for diodes and ion chambers in small photon fields," Phys. Med. Biol. **58**, 2431–2444 (2013).
[22]A. Wagner, F. Crop, T. Lacornerie, F. Vandevelde, and N. Reynaert, "Use of a liquid ionization chamber for stereotactic radiotherapy dosimetry," Phys. Med. Biol. **58**, 2445–2459 (2013).
[23]H. Benmakhlouf, J. Sempau, and P. Andreo, "Output correction factors for nine small field detectors in 6 MV radiation therapy photon beams: A PENELOPE Monte Carlo study," Med. Phys. **41**, 041711 (12pp.) (2014).
[24]J. Wulff, J. T. Heverhagen, and K. Zink, "Monte-Carlo-based perturbation and beam quality correction factors for thimble ionization chambers in high-energy photon beams," Phys. Med. Biol. **53**, 2823–2836 (2008).
[25]K. Zink and J. Wulff, "On the wall perturbation correction for a parallel-plate NACP-02 chamber in clinical electron beams," Med. Phys. **38**, 1045–1054 (2011).
[26]L. A. Buckley and D. W. Rogers, "Wall correction factors, Pwall, for thimble ionization chambers," Med. Phys. **33**, 455–464 (2006).
[27]H. Bouchard, J. Seuntjens, J. F. Carrier, and I. Kawrakow, "Ionization chamber gradient effects in nonstandard beam configurations," Med. Phys. **36**, 4654–4663 (2009).
[28]F. Crop, N. Reynaert, G. Pittomvils, L. Paelinck, C. De Wagter, L. Vakaet, and H. Thierens, "The influence of small field sizes, penumbra, spot size and measurement depth on perturbation factors for microionization chambers," Phys. Med. Biol. **54**, 2951–2969 (2009).
[29]A. S. Beddar, T. R. Mackie, and F. H. Attix, "Water-equivalent plastic scintillation detectors for high energy beam dosimetry: II. Properties and measurements," Phys. Med. Biol. **37**, 1901–1913 (1992).
[30]A. S. Beddar, T. R. Mackie, and F. H. Attix, "Water-equivalent plastic scintillation detectors for high energy beam dosimetry: I. Physical characteristics and theoretical consideration," Phys. Med. Biol. **37**, 1883–1900 (1992).
[31]P. Francescon, S. Cora, C. Cavedon, and P. Scalchi, "Application of a Monte Carlo-based method for total scatter factors of small beams to new solid state micro-detectors," J. Appl. Clin. Med. Phys. **10**(1), 147–152 (2009).
[32]E. Pantelis, C. Antypas, L. Petrokokkinos, P. Karaiskos, P. Papagiannis, M. Kozicki, E. Georgiou, L. Sakelliou, and I. Seimenis, "Dosimetric characterization of CyberKnife radiosurgical photon beams using polymer gels," Med. Phys. **35**, 2312–2320 (2008).
[33]D. W. Rogers, B. A. Faddegon, G. X. Ding, C. M. Ma, J. We, and T. R. Mackie, "A Monte Carlo code to simulate radiotherapy treatment units," Med. Phys. **22**, 503–524 (1995).
[34]I. Kawrakow, E. Mainegra-Hing, F. Tessier, and B. R. B. Walters, "The EGSnrc c++ class library," Report PIRS 898 (Ottawa, Canada) (rev A).
[35]J. Wulff, K. Zink, and I. Kawrakow, "Efficiency improvements for ion chamber calculations in high energy photon beams," Med. Phys. **35**, 1328–1336 (2008).
[36]L. A. Buckley, I. Kawrakow, and D. W. Rogers, "An EGSnrc investigation of cavity theory for ion chambers measuring air kerma," Med. Phys. **30**, 1211–1218 (2003).
[37]J. Morin, D. Beliveau-Nadeau, E. Chung, J. Seuntjens, D. Theriault, L. Archambault, S. Beddar, and L. Beaulieu, "A comparative study of small field total scatter factors and dose profiles using plastic scintillation detectors and other stereotactic dosimeters: The case of the CyberKnife," Med. Phys. **40**, 011719 (11pp.) (2013).
[38]L. L. Wang and S. Beddar, "Study of the response of plastic scintillation detectors in small-field 6 MV photon beams by Monte Carlo simulations," Med. Phys. **38**, 1596–1599 (2011).
[39]J. C. Gagnon, D. Theriault, M. Guillot, L. Archambault, S. Beddar, L. Gingras, and L. Beaulieu, "Dosimetric performance and array assessment

of plastic scintillation detectors for stereotactic radiosurgery quality assurance," Med. Phys. **39**, 429–436 (2012).
[40]D. M. Klein, R. C. Tailor, L. Archambault, L. Wang, F. Therriault-Proulx, and A. S. Beddar, "Measuring output factors of small fields formed by collimator jaws and multileaf collimator using plastic scintillation detectors," Med. Phys. **37**, 5541–5549 (2010).
[41]H. Bouchard, J. Seuntjens, and I. Kawrakow, "A Monte Carlo method to evaluate the impact of positioning errors on detector response and quality correction factors in nonstandard beams," Phys. Med. Biol. **56**, 2617–2634 (2011).
[42]F. Verhaegen, I. J. Das, and H. Palmans, "Monte Carlo dosimetry study of a 6 MV stereotactic radiosurgery unit," Phys. Med. Biol. **43**, 2755–2768 (1998).